Separation and Purification Technology 344 (2024) 127268

Contents lists available at ScienceDirect

Separation and Purification Technology

journal homepage: www.elsevier.com/locate/seppur

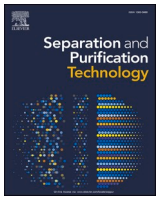

Enhanced toluene adsorption over carbon–silica composite with promoted microporosity and moisture resistance

Quanli Ke [a], Yedong Xiong [a], Mei Lu [b], Guonan Fang [a], Guokai Cui [a], Pengyun Pan [a], Feng Xiong [a], Tianhao Wu [b], Kangkang Huang [b], Jiong Min [c], Chuanmin Jin [c], Hanfeng Lu [a,*]

[a] Institute of Catalytic Reaction Engineering, College of Chemical Engineering, Zhejiang University of Technology, Hangzhou 310014, PR China
[b] Zhejiang Environmental Technology Co., Ltd., Hangzhou 311121, PR China
[c] Joint Research Center with ZJUT, Zhejiang Yuesheng Environmental Technology Co., Ltd., Huzhou 313300, PR China

ARTICLE INFO

Handling Editor: Z Bao

Keywords:
Carbon-silica composites
Microporosity
Adsorption-desorption properties
Moisture resistance
VOCs adsorption

ABSTRACT

Herein, carbon–silica composite materials were prepared by introducing biomass-derived carbon into the channels of silica gel by concurrent thermal carbonization and chemical etching. With the optimized preparation parameters, a trade-off for the microporosity, carbon contents and toluene adsorption capacity was realized. Moreover, the TEM-EDS spectra evidenced that the carbon generated by chemical activation was homogeneously dispersed in the channels of the silica gel. Notably, when used in toluene adsorption, high adsorption capacity, desorption efficiency and regenerability were simultaneously achieved on the carbon–silica composite sample, along with superb water resistance (up to 80 RH%), as contrasted with the performances of the commercial zeolite adsorbents. Finally, except for the toluene, the composite material demonstrated good adsorption capacity and desorption efficiency for a series of common VOCs species (including acetone, ethyl acetate, n-hexane) as well, but the adsorption towards less polar adsorbates, such as n-hexane and toluene, was more favorable.

1. Introduction

Volatile organic compounds (VOCs), as one of the main air pollution sources, have received intensive attentions recently. These organic contaminants not solely cause toxic effects on human bodies and increase the risks of respiratory disease or even cancer, but also contribute to the ozone production and therefore generate secondary air pollution [1–3]. In order to relieve the severe harms of VOCs pollutants, numerous measures have been put forward hitherto, which could be mainly divided into two categories, namely the elimination and the recovery methods. The elimination methods include thermal oxidation, catalytic combustion, photocatalysis, biodegradation, plasma oxidation, etc., which normally convert the VOCs into final harmless CO_2 and H_2O [4–9]. Therein, the thermal oxidation method easily causes concerns about the energy consumption, while the catalytic combustion also suffers from the catalyst deactivation, especially the noble-metal catalysts[2,10]. In the meantime, the large-scale applications of photocatalysis, biodegradation and plasma oxidation are severely restricted by the long-term efficiency, strict operation environment and secondary pollution, respectively, in practical scenarios[11–14]. The prevalent recovery methods include the adsorption, absorption, condensation and membrane separation. However, the absorption way always requires a large amount of solvent, which gives rise to the problems of solvent recovery, whereas the condensation is more suitable for high-concentration occasions and brings about the high manufacture investment[15–17]. Moreover, although high selectivity and recovery rate could be simultaneously fulfilled by the membrane separation, the high energy consumption, low gas flux and inferior stability subject to complicated contaminants remain the tough issues in this approach [18,19]. With these concerns, adsorption seems a more attractive solution in consideration of its low energy cost, feasible operation, fast kinetics and low risks of external contamination[20–22].

Adsorbent is the key to the adsorption process, which imparts a significant influence on the capacity, selectivity and energy penalty. Typically, there are two main driving forces in the scope of VOCs adsorption, the electrostatic attraction and the molecule-pore wall interaction (including both hydrophobic and hydrophilic surfaces), which are closely associated with the electric field intensity and the textural properties (surface area and pore size) within the adsorbents, respectively[21–23]. Given the non-polar nature of the VOCs molecules,

* Corresponding author.
E-mail address: luhf@zjut.edu.cn (H. Lu).

https://doi.org/10.1016/j.seppur.2024.127268
Received 3 February 2024; Received in revised form 18 March 2024; Accepted 26 March 2024
Available online 27 March 2024

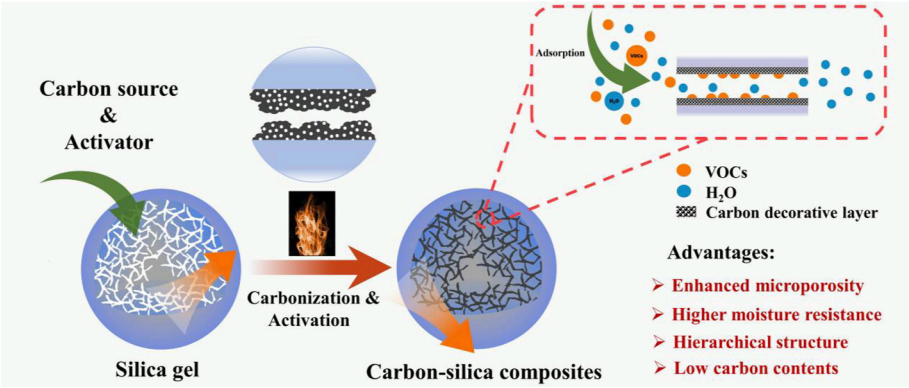

Scheme 1. The preparation of carbon–silica composite with promoted microporosity and moisture resistance by a concurrent thermal carbonization and chemical etching method.

the molecule-pore wall interaction is obviously more favorable for the VOCs molecules capture. Therefore, a series of porous materials are then synthesized and functionalized to obtain narrower pore aperture (size < 0.7 nm) and higher surface area. Among the porous materials, activated carbons (ACs), metal–organic frameworks (MOFs) (including the MOFs-derived carbon materials), covalent organic frameworks (COFs) and zeolites are preferred for their uniformly small pore diameters and high specific surface areas, which induces stronger appeal of their pore walls to the adsorbates[20,24–31]. Nonetheless, the thermolabile structure of ACs may easily result in safety issues like spontaneous burning, while MOFs and COFs also face some drawbacks such as tricky synthesis, high manufacture expense and low stability subject to water/steam/high temperature, which badly interfere with their potential applications [29,32]. In this consideration, zeolite could be a promising adsorbent material for its excellent chemical stability, tunable pore size, and unique ion exchange properties, which has already been widespreadly used in industrial rotary adsorption equipment[20]. However, the intrinsic microporous feature of zeolite results in problems such as difficulty in desorption and inferior moisture resistance as well[27]. Although the increase of silica contents could strengthen the moisture resistance of zeolites, the high functionalization expense on zeolites further limits their up-scaled usage[33]. Thereby, it is urgently necessitated to seek for an alternative adsorbent with higher desorption efficiency, enhanced moisture resistance, and lower manufacture cost.

Compared to the aforementioned microporous adsorbents, silica gel is a more conventional adsorbent, of which the high porosity, thermal stability and mechanical strength render it an intriguing backbone for the alternative adsorbent. Yet the presence of abundant surface silanol groups results in its strong water affinity and then competitive adsorption between moisture and VOCs molecules. Provided the hydrophobic nature of ACs, as witnessed by their applications in aqueous treatments [30,31], the decoration of silica precursor by ACs, that is, the carbon–silica composite, could be a promising way to couple their merits, *i.e.* the silica backbone could ensure the thermal stability, while the carbon layer promote both the porosity and moisture resistance. Previously, we have summarized the state of the art in the preparation routes, structure–function relationship and applications of the carbon–silica composite material[34]. As for the applications in adsorption, several reports have disclosed the preparation of nanoporous carbon–silica composites by encapsulating the ACs powder into the silica aerogel, which could realize both high adsorption capacity and desorption efficiency for VOCs including n-hexane and benzene[35,36]. Besides, Han et al. have prepared a carbon–silica composite by the tandem extrusion forming and thermal treatment, which exhibited excellent adsorption–desorption performances towards p-xylene, along with an increased ignition temperature (>40℃) compared to the ACs[37]. Even though the thermal stability of the carbon–silica composites in the aforementioned works could be indeed enhanced, the moisture resistance during the adsorption processes was rarely discussed (or explored under low RH%). Recently, our group have also reported the fabrication of carbon–silica composite with hierarchical porous structure by introducing the biomass precursor into the silica channels, followed by hydrothermal carbonization and calcination[38]. As a consequence, the adsorption capacity for a series of VOCs has been improved on the composite when compared to the silica, even with relative humidity up to 80 %. Even though some progresses have already been made in the carbon–silica composite synthesis, it should be noted that some bottlenecks are still remaining, for instance, the cumbersome synthesis procedure, pore blocking by coke, and inferior overall adsorption capacity.

Herein, a facile strategy for preparing carbon–silica composite with hierarchical porous structure was proposed, where silica gel was adopted as silica precursor and sucrose as carbon source (Scheme 1). Subject to chemical etching under high temperature, the fraction of micropores in the final composite was greatly enhanced when compared to the original silica gel, leading to the enhanced adsorption force between the pore wall and VOCs molecules. Meanwhile, a trade-off between the adsorption performance and desorption efficiency could be realized by using this composite material, which maintained high toluene adsorption capacity up to 5 adsorption–desorption cycles. Taking advantage of the inherent hydrophobicity of the carbon layer, the composite material also exhibited remarkable water resistance, as evidenced by its less significant decline of dynamic adsorption capacity under increased humidity. Next to that, with the protection of silica gel, the composite material showed a high ignition temperature, which translates to its good thermal stability. Therefore, this new carbon–silica composite materials could be a superb candidate for the highly efficient removal of VOCs in practice.

2. Experimental

2.1. Chemical and materials

Toluene (SCR Co. Ltd; >99.5 %), n-Hexane (Shanghai Lingfeng Chemical; >97 %), Acetone (Shanghai Taitan Scientific; >99.5 %), Ethyl acetate (Shanghai Taitan Scientific; >99.5 %), Sucrose (SCR Co. Ltd; AR grade), Zinc chloride (Macklin; 98 %), B-type silica gel (Qingdao Shuoyuan Silica Technology Co., Ltd.), hydrochloric acid (SCR Co. Ltd; 36–38 %). NaY (SiO_2/Al_2O_3 = 5.5; Nkcatalyst), Naβ (SiO_2/Al_2O_3 = 26; Nkcatalyst), ZSM-5 (Na-type, SiO_2/Al_2O_3 = 26; Nkcatalyst). All chemicals of analytical grade were used as received without further treatments.

2.2. Preparation of carbon–silica composite

The carbon–silica composite samples were prepared as follows. A

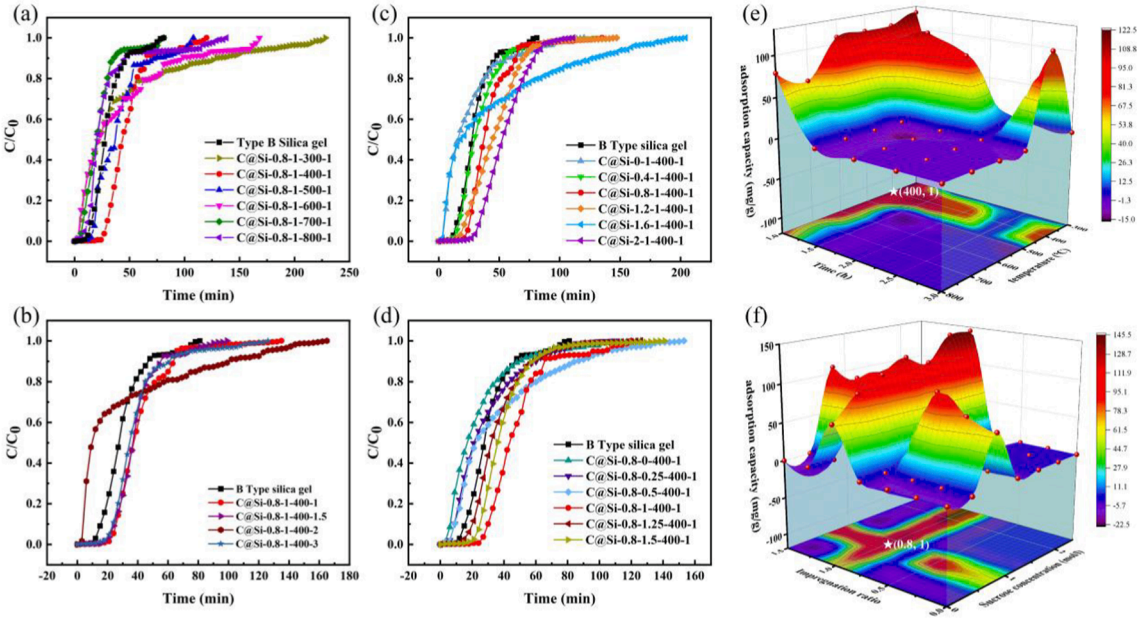

Fig. 1. Toluene adsorption breakthrough curves of carbon–silica composite samples prepared under different preparation conditions: (a) calcination temperature (b) calcination time (c) sucrose concentration (d) impregnation ratio. The visual presentation for the influences of (e) calcination time and calcination temperature and (f) impregnation ratio and sucrose concentration on the toluene adsorption capacities, basing on the breakthrough curves in Fig. 1 (a-d) (The inlet toluene concentration was 10000 mg/m^3, the flow rate was maintained at 83.3 mL·min^{-1}, and the weight hourly space velocity was kept at 16660 mL/g·h).

certain amount of sucrose (as the carbon source) and zinc chloride (as the activator for thermal carbonization) were first mixed in 10 g of deionized water. The sucrose precursor was adopted because of its high carbon contents, superb solubility and low cost. The hydrochloric acid was then added dropwise into the solution above to adjust the pH value, and the resulting mixture was stirred continuously until a transparent solution was obtained. Subsequently, different amounts of the transparent solution were introduced into 3 g of B-type silica gel by incipient wetness impregnation method so as to achieve different impregnation ratios (mass ratio of zinc chloride to sucrose). The mixture was kept at room temperature for 10 h and then dried at 45℃ for 12 h. Thereafter, the dried powder was transferred into a tubular furnace and calcined in N_2 atmosphere under varied temperatures (N_2 flow100 ml/min, heating rate 10℃/min, the calcination time was counted after the temperature ramped to the target values). Some caramel-like species were observed in the early stage of the thermal treatments, which were further carbonized with the assistance of zinc chloride activator, as shown in **Figure S3.5**. After calcination, the samples were washed using 0.1 mol/L HCl solution (50 mL) for 3 times, and using deionized water until the pH values got neutral, so as to remove the residual zinc chloride and avoid its possible interaction with toluene and moisture. Finally, the samples were dried at 110℃ for 12 h and the obtained carbon–silica composite samples were denoted as C@Si-A-B-C-D, where A represents the concentration of sucrose, B represents the impregnation ratio, C represents the calcination temperature (℃) and D represents the calcination time (hour).

2.3. The dynamic desorption & cyclic adsorption test procedure

The dynamic adsorption test was conducted in a continuous-flow fixed-bed reactor at atmospheric pressure. In each test, 0.3 g of adsorbents was placed in the U-shaped tube reactor. The toluene feed gas was generated by bubbling the VOCs (toluene, acetone, ethyl acetate, etc.) liquids with air in an ice-water bath. The VOCs-containing feed gas was then diluted by certain air flow so that the total flow rate was maintained at 83.3 mL·min^{-1} (toluene concentration = 10000 mg/m^3, weight hourly space velocity = 16660 mL/g·h). In case of the humidity-resistant tests, a third gas flow was generated by bubbling the liquid water with air in a 25℃ thermostat water bath and mixed with the aforementioned VOCs-containing feed gas, so as to form the final VOCs-containing feed gases with different relative humidity (0 %, 40 %, 60 %, 80 %). Thereafter, the final feed gases were injected into the U-shaped tube immersed in a 25℃ thermostat water bath for adsorption tests. The concentrations of VOCs were continuously measured by automatic sampling into a gas chromatography (Agilent 6890) equipped with a flame ionization detector (FID) and HP-5 column. Meanwhile, the mass before and after the dynamic adsorption tests were both recorded so as to calibrate the VOCs adsorption capacity. The detailed procedure of the dynamic adsorption tests was shown in **Figure S1.1**. The VOCs adsorption capacity was calculated by the following equation:

$$q_a = \frac{F \times C_0 \times 10^{-6}}{W}\left[t_s - \int_0^{t_s} \frac{C_i}{C_0} dt\right]$$

where q_a is the adsorption capacity, mg/g; t_s is the time when adsorption equilibrium was reached, min; F is the total gas flow, 83.3 mL/min; W is the mass of the adsorbents, g; C_0 is the inlet VOCs mass concentration, mg/m^3, and Ci is the outlet mass concentration, mg/m^3.

The dynamic desorption test was conducted in the same fixed-bed reactor via a similar procedure. Instead of the VOCs-containing feed gases, the air flow (flow rate: 83.3 mL·min^{-1}) was injected into the U-shaped tube immersed in a 60℃ thermostat water bath for desorption tests. The desorption tests were terminated when the VOCs signals detected by the gas chromatography got convergent, which means the desorption equilibrium has been reached. The mass before and after the dynamic desorption tests were both recorded to calculate the VOCs desorption capacity and efficiency, according to the following equations:

$$q_d = \frac{m_a - m_d}{m_0} \times 1000$$

$$\eta = \frac{m_a - m_d}{m_a - m_0}$$

where q_d is the desorption capacity, mg/g; m_0 is the initial adsorbent mass; m_a is the adsorbent mass when the adsorption equilibrium was

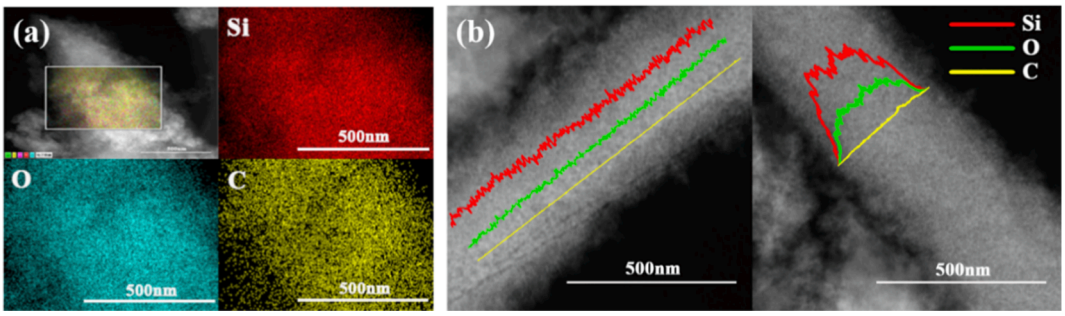

Fig. 2. (a) The corresponding element (Si, O and C) distribution and (b) line scan diagram of C@Si composite.

reached, g; m_d is the adsorbent mass when the desorption equilibrium was reached, g.

The cyclic adsorption tests were conducted by the following procedure: the samples were first subject to the dynamic adsorption tests for 90 mins under 25℃ (stopped before saturation for efficiency consideration), and then desorbed under 60℃ until equilibrium was reached (*ca.* 2 h). Thereafter, the same procedure was performed on the regenerated samples, and the cyclic adsorption capacity was defined as the capacity obtained after different times of regeneration.

2.4. Characterizations

The properties of the carbon–silica composite were characterized using a series of techniques, such as nitrogen adsorption–desorption isotherms at 77 K, thermogravimetric analysis, field emission scanning electron microscopy (FE-SEM), and high resolution transmission electron microscopy (HRTEM) equipped with elemental analysis. The detailed characterization procedures and parameters can be seen from the Supporting information.

3. Results and discussion

3.1. The synthesis condition screening

Since the adsorption performances of the carbon–silica composites greatly rely on their preparation conditions, a screening for the synthesis parameters was first conducted, including the calcination temperature (300-800℃), calcination time (1–3 h), sucrose concentration (0.1–2 mol/L) and impregnation ratio (0–1.5). According to the dynamic adsorption tests results, the toluene adsorption capacities on most of the carbon–silica composite samples were obviously higher than that on the pristine B-type silica, which evidenced the benefits of the carbon decoration onto the silica gel (Fig. 1**a-d**). Specifically, with increased activation temperatures, the adsorption capacities of the composite materials generally showed a decreasing trend (Fig. 1**a**, Table S2.2). Since the surface area and pore size distribution (PSD) are crucial for the VOCs adsorption properties, the N_2 adsorption–desorption isotherms were then collected on the composite materials. As shown, the hysteresis loop gradually disappeared with the temperature increase, which translated to declined microporous area and volume (Figure S2.1, Table S2.1). Moreover, the pore size of the carbon–silica composite samples displayed a centered distribution at *ca.* 2 nm as well as lower mesopore fraction in 4–10 nm up to 600℃, which validated the successful introduction of carbon into the silica pore and the consequent pore size adjustment (Figure S2.2). However, when the calcination temperature was higher than 600℃, the PSD moved to even smaller region while the original mesopore totally disappeared, which could be related to the pore shrinkage. Because the carbon layer significantly affects the moisture resistance and thermal stability of the composite materials, the weight loss and resultant carbon contents were then plotted against the calcination temperature (Figure S2.3-2.4). Accordingly, a remarkable weight loss was witnessed in 500-700℃, which fitted well with the decreasing carbon contents and micropores. According to our previous researches, the contents should be maintained below 15 wt% so that the safety issues could be avoided during the exthermal VOCs adsorption process. Meanwhile, too little carbon contents can hardly cover all the surface silanol groups and weaken the moisture affinity. In this consideration, the calcination temperature of 400℃ could be an appropriate choice, where a balance for the capacity and carbon content could be concurrently realized. Likewise, several other important preparation parameters (calcination time, sucrose concentration and impregnation ratio) were also screened (Figure S2.5-2.16, Table S2.3-2.8). In summary, the optimal preparation conditions are calcination temperature at 400 °C, calcination time for 1 h, impregnation ratio of 1 and sucrose concentration of 0.8 mol/L (Fig. 1**e-f**). The corresponding sample was denoted as C@Si-0.8–1-400–1, which was abbreviated to C@Si in the following context for convenience.

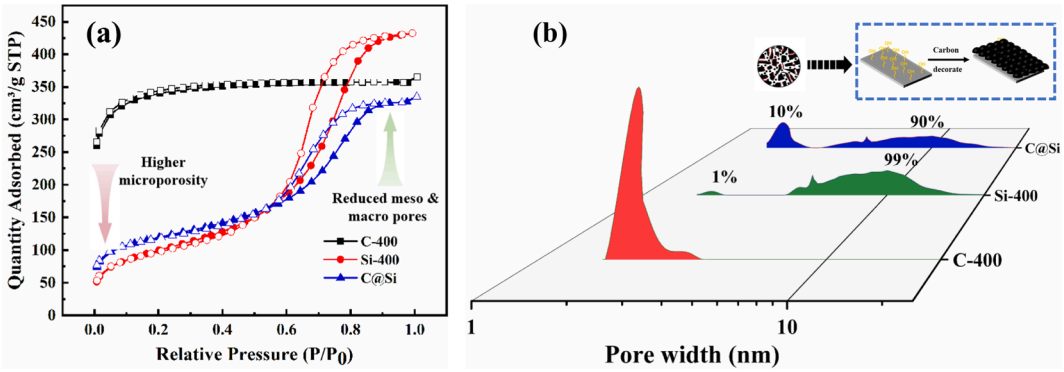

Fig. 3. (a) N_2 adsorption–desorption isotherms at 77 K and (b) pore size distribution of C@Si, activated carbon (C-400) prepared under same condition and B-type silica (Si-400) treated under the same calcination temperature.

Table 1
Textural properties parameters of the samples.[a].

Sample	S_{BET} (m^2/g)	S_{Mic} (m^2/g)	V_{Total} (cm^3/g)	V_{Mic} (cm^3/g)
C-400	1269.5	1163.2	0.5536	0.4847
Si-400	349.1	0	0.6656	0
C@Si	431.1	136.7	0.5073	0.0520

[a] The textual properties were all obtained from the adsorption isotherms. The linearity of fitting for the BET specific surface area (S_{BET}) was 0.99999; Total pore volume (V_{Total}) was calculated by Gurvich-rule at $P/P^0 = 0.95$; Microporous volume (V_{Mic}) and microporous surface area (S_{Mic}) was calculated by t-Plot method.

3.2. Textural characteristics

To investigate the change of the silica after carbon modification, the morphologies of both the original silica and the C@Si composite were then examined. According to **Figure S3.1**, there are no apparent differences or carbon microspheres detected in these two samples, which indicates the encapsulation of carbon in the silica channels. In order to verify this phenomenon, the TEM-EDS mapping was conducted, wherein the three elements (Si, O, and C) are uniformly dispersed (Fig. 2**a**). Furthermore, two regions of the C@Si sample were scanned in line-scan mode. Interestingly, the factions of all three elements kept constant in the axial direction but showed bell-shaped distributions in the radial direction (because of the greater pore-wall thickness in the middle), which well reflects the homogeneous distributions of carbon contents in the porous structure of the silica gel **(**Fig. 2**b)**. Next to that, the (D)TGA tests were also conducted to check the thermal stability of the C@Si composite sample. As shown, a great carbon weight loss was witnessed at temperature higher than 500℃, which clearly proves the remarkable thermal resistance of the composite sample (**Figure S3.2**).

It is mentioned above that the introduction of carbon would have a great impact on the adsorption capacity. As benchmarks, the sucrose and silica gel precursors were treated under the same preparation conditions and calcination temperature, respectively, with those of the C@Si composite (denoted as C-400 and Si-400). Fig. 3**a** depicts the nitrogen adsorption–desorption isotherms and PSDs of the three samples. Therein, Si-400 and C@Si both exhibit type-IV isotherms and H1-type hysteresis loops, which suggests the existence of mesopores; however, the C-400 sample exhibits type-I isotherm, which refers to the dominance of micropores **(**Fig. 3**a)**. Notably, the C@Si composite sample demonstrates higher N_2 filling in the low pressure region but lower amount in the high pressure region, when compared to the original silica gel, proving the enhanced micropore in the former sample at the expense of macro(meso)pores (Fig. 3**a,** Table 1**)**. Furthermore, a great increase (10 times higher than that of Si-400) of the micropore fraction was observed in the PSD of C@Si composite along with the deteriorated mesopore proportion (Fig. 3**b**). Since the C@Si composite and C-400 both showed centered PSDs at 2 nm, it evidenced that the decoration of silica gel by biomass-derived carbon could indeed modify its pore size and generate a more hierarchical porous structure therein (the so-called hierarchical structure is comprised of the new micropore with 2 nm size associated with the carbon introduced, and the intrinsic mesopore in silica gel), which is quite beneficial to its adsorption performances.

3.3. Dynamic adsorption, desorption and regeneration tests towards toluene

To evaluate the adsorption performances of the obtained composite sample, the dynamic adsorption–desorption experiments towards toluene were performed on it with comparison to the pristine silica gel and several most common commercial zeolites. As shown in Fig. 4**a**, the penetration time of C@Si was obviously longer than that of B-type silica gel, which proves that the micropores generated by carbon modification enhanced both the adsorption capacity and toluene affinity of silica gel. When compared to the most widespread zeolites adsorbents (NaY, Naβ and ZSM-5), it was also found that the adsorption affinity of NaY and ZSM-5 was much weaker, as proven by the rapid breakthrough and slow ascending trend in their dynamic toluene adsorption curves (Fig. 4**a**). Except for the adsorption capacity, the desorption efficiency is another important parameter. Markedly, while the C@Si composite showed comparable toluene adsorption capacity to those of commercial zeolites, the remaining toluene in C@Si after desorption was also much lower (*ca.* 18.5 % residual), which means better desorption efficiency in the C@Si sample **(**Fig. 4**b,** Table 2**)**. This advantage could also be attributed to the hierarchical porous structure of the C@Si composite sample, wherein the diffusion rate of toluene is faster than that in the ultra-microporous channels of zeolites.

Provided the high adsorption capacity and desorption efficiency of

Table 2
The adsorption–desorption capacities of different samples.

Sample	Adsorption capacity (mg/g)	Desorption capacity (mg/g)
B Type silica	84.0	54.5
C@Si	110.0	89.7
NaY	104.1	23.8
Naβ	112.2	30.3
ZSM-5	59.7	18.6

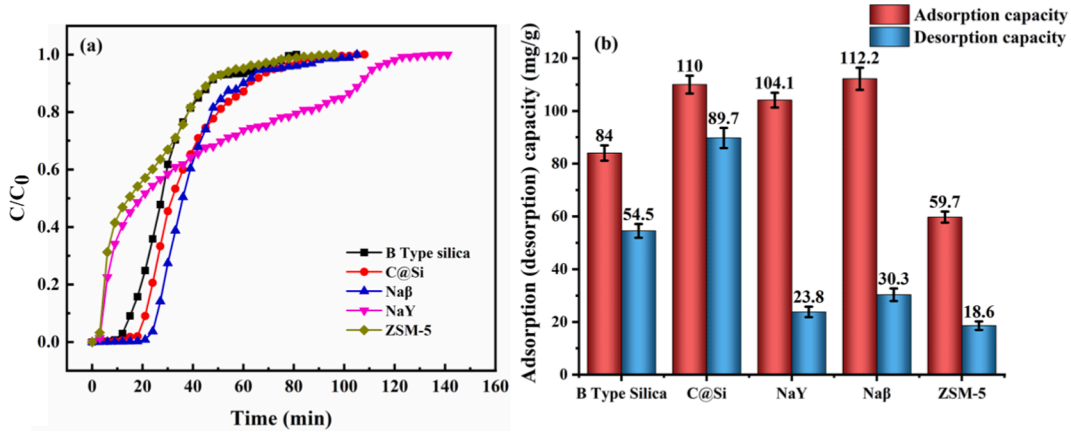

Fig. 4. (a) Toluene adsorption breakthrough curves of B-type silica, C@Si and commercial zeolites under dry condition and (b) adsorption–desorption capacity of C@Si in comparison to those of commercial zeolites. (The inlet toluene concentration was 10000 mg/m^3, the flow rate was maintained at 83.3 mL·min^{-1}, and the weight hourly space velocity was kept at 16660 mL/g·h. The desorption capacity was defined as the amount of toluene that could depart from the adsorbents after desorption equilibrium was reached under 60℃, which corresponds to the adsorption capacity.).

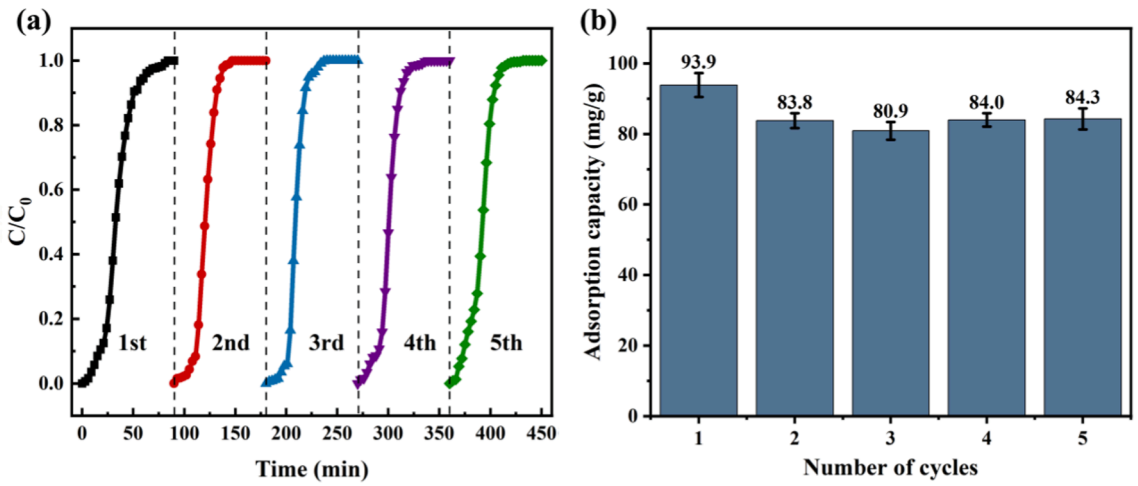

Fig. 5. (a) The cyclic adsorption breakthrough curves and (b) cyclic adsorption capacity of toluene on C@Si. The cyclic adsorption was performed as follows: the C@Si sample was first saturated at 25℃ and then regenerated at 60℃ till the equilibrium was reached. The cyclic adsorption capacity was defined as the capacity obtained after different times of regeneration. The 1st cycle means the adsorption using fresh C@Si sample, but the dynamic adsorption tests were stopped after 90 mins for efficiency consideration, see more details in Section 2.3.

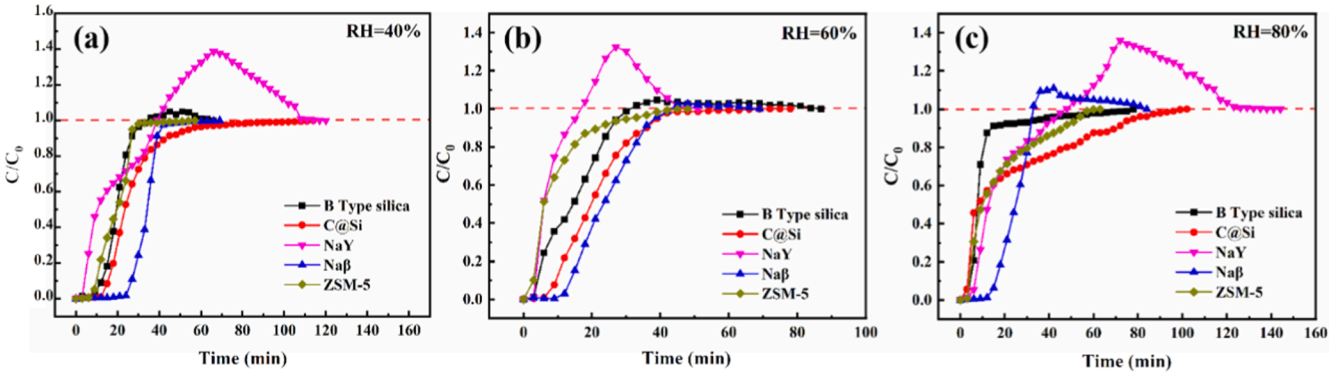

Fig. 6. Toluene adsorption curves of sample under (a) 40 RH%, (b) 60 RH% and (c) 80 RH%. (The inlet toluene concentration was 10000 mg/m^3, the flow rate was maintained at 83.3 mL·min^{-1}, and the weight hourly space velocity was kept at 16660 mL/g·h.).

the C@Si composite sample, the cyclic adsorption tests were conducted to investigate the regeneration stability of the composite sample. To avoid the deterioration of the carbon layer under high temperature, the samples was first saturated at 25℃ and then thermally activated at 60℃ till the equilibrium was reached, followed by repeats for 5 cycles. The toluene adsorption breakthrough curves were collected after each cycle to assess the regenerability of the composite. Accordingly, albeit there was a small capacity decrease from 93.9 mg/g (it is smaller than the toluene capacity in Table 2 because the adsorption time was kept at 90 mins) to 83.8 mg/g after the first cycle, the subsequent capacity maintained at approximate values, which explicitly manifests the superior regenerability of the composite (Fig. 5).

3.4. Water resistance test

As per above, the inferior moisture resistance is another severe problem that needs to be addressed, since the adsorbents have to capture the VOCs molecules under humid conditions in the reality. Therefore, water resistance is also an important index for a qualified adsorbent. As shown in Fig. 6, the toluene breakthrough tests under a series of humidity were performed on the C@Si composite sample, and its performance was compared with those of B-type silica gel and commercial zeolites. It is worth noting that while the adsorption capacity of the C@Si composite sample retained at 63.4 mg/g even under 80 % RH, those of the B-type silica and commercial zeolites (especially NaY and Naβ) decline markedly with the increase of humidity, along with fierce competitive adsorption of the water molecules (Fig. 6, Table 3). In order to verify the moisture resistance of the C@Si composite sample more straightforwardly, the water contact angles were measured for both the C@Si composite and the Si-400 benchmark sample. As shown, an obviously larger water contact angle was witnessed in the C@Si composite sample, as a consequence of carbon layer decoration (**Figure S3.3-3.4**). These results proves that the carbon modification of the silica gel could strengthen its moisture resistance, which makes the C@Si composite sample an excellent candidate for VOCs capture in humid environment.

Table 3
The summarization of dynamic toluene adsorption capacity of samples under different humidity.

Sample	Adsorption capacity (mg/g)		
	RH = 40 %	RH = 60 %	RH = 80 %
B Type silica	49.5	35.6	29.4
C@Si	73.9	66.2	63.4
NaY	6.2	4.4	0.55
Naβ	92.5	65.4	22.2
ZSM-5	52.6	52.2	47.3

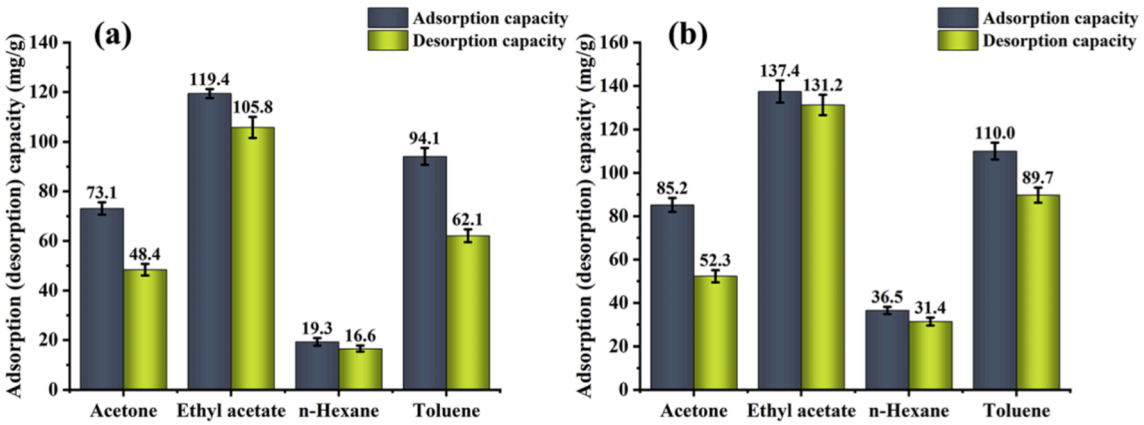

Fig. 7. The adsorption and desorption capacity of (a) B type silica and (b) C@Si toward acetone, ethyl acetate, n-hexane and toluene. The desorption capacity was defined as the amount of toluene that could depart from the adsorbents after desorption equilibrium was reached under 60°C, which corresponds to the adsorption capacity.

3.5. Extension to adsorption toward diverse VOCs

In the practical circumstances, the exhaust gas is seldom comprised of sole VOCs but diverse varieties. In order to have a comprehensive evaluation of the adsorption properties of the C@Si composite sample, the dynamic adsorption–desorption experiments towards several other VOCs molecules (acetone, ethyl acetate, n-hexane) were also performed and confronted with those of the original silica gel (Fig. 7). Generally, the composite exhibited more remarkable adsorption capacity for all three VOCs, but the increment for the VOCs with smaller dipole moments (n-hexane and toluene) was obviously more prominent (**Table S3.1**). With regard to the desorption efficiency, the desorbed proportions of toluene and ethyl acetate were both higher on the C@Si composite than those on the silica gel, whereas the desorbed proportions of n-hexane and acetone more or less parallel. This point indicates that there may exist an optimal polarity region (neither too high nor too low) for the VOCs adsorbates to have an appropriate affinity with the adsorbent surface. Notably, the C@Si composite sample had both excellent adsorption capacity and desorption efficiency for ethyl acetate, reaching up to 137.4 mg/g and 95.5 %, respectively, which could then serve as a promising adsorbent for the exhaust gas treatment in coating and printing processes.

4. Conclusion

As described, a carbon–silica composite with hierarchical porous structure was prepared by introducing sucrose into the silica precursor as carbon source, followed by chemical etching under high temperature. After the preparation parameters optimization, this composite material with homogeneously dispersed carbon contents showed superior microporosity to that of the pristine silica gel and consequently better toluene adsorption capacity. Next to that, this novel composite material also demonstrated excellent adsorption capacity, desorption efficiency, regenerability and moisture resistance (up to 80 RH%), when compared to the most widespread commercial zeolites. Finally, to have a comprehensive understanding of the adsorption properties towards diverse VOCs species, the corresponding dynamic adsorption–desorption tests were then conducted on the C@Si composite. The results showed that the composite had generally higher adsorption capacity, particularly for the VOCs with weaker polarity, as compared to the performances of the original silica gel, while the desorption efficiency depended on the polarity of the VOCs. This novel and facile synthesis strategy for the highly qualified carbon–silica composite adsorbent presents a new method for the functionalization of macroporous materials, and a range of relevant exhaust abatement applications could now be explored.

CRediT authorship contribution statement

Quanli Ke: Writing – review & editing, Writing – original draft, Supervision, Funding acquisition. **Yedong Xiong:** Investigation, Data curation. **Mei Lu:** Data curation, Investigation, Project administration. **Guonan Fang:** Investigation, Data curation. **Guokai Cui:** Funding acquisition, Methodology. **Pengyun Pan:** Investigation, Data curation. **Feng Xiong:** Investigation, Data curation. **Tianhao Wu:** Investigation, Writing – original draft. **Kangkang Huang:** Investigation, Data curation. **Jiong Min:** Funding acquisition. **Chuanmin Jin:** Funding acquisition. **Hanfeng Lu:** Supervision, Methodology, Funding acquisition, Conceptualization.

Declaration of competing interest

The authors declare that they have no known competing financial interests or personal relationships that could have appeared to influence the work reported in this paper.

Data availability

Data will be made available on request.

Acknowledgments

This study was financially supported by the Natural Science Foundation of China (grant number: 22208300, 22078294), Natural Science Foundation of Zhejiang Province (grant number: LQ23B060007), Fundamental Research Funds for the Provincial Universities of Zhejiang (grant number: RF-A2023004), Zhejiang Provincial Postdoctoral Science Foundation (grant number: ZJ2023145), Key Research and Development Projects in Zhejiang Province (grant number: 2023C03127, 2024C03108)

Appendix A. Supplementary data

Supplementary data to this article can be found online at https://doi.org/10.1016/j.seppur.2024.127268.

References

[1] L. Zhang, X. Li, H. Chen, et al., Haze air pollution health impacts of breath-borne VOCs[J], Environ. Sci. Technol. 56 (12) (2022) 8541–8551.
[2] C. He, J. Cheng, X. Zhang, et al., Recent advances in the catalytic oxidation of volatile organic compounds: a review based on pollutant sorts and sources[J], Chem. Rev. 119 (7) (2019) 4471–4568.

[3] Q. Li, G. Su, C. Li, et al., An investigation into the role of VOCs in SOA and ozone production in Beijing, China[J], Sci. Total Environ. 720 (2020) 137536.
[4] Y. Zheng, Y. Su, C. Pang, et al., Interface-enhanced oxygen vacancies of CoCuOx catalysts in situ grown on monolithic cu foam for VOC catalytic oxidation[J], Environ. Sci. Technol. 56 (3) (2022) 1905–1916.
[5] F. Bi, X. Feng, Z. Zhou, et al., Mn-based catalysts derived from the non-thermal treatment of mn-MIL-100 to enhance its water-resistance for toluene oxidation: mechanism study[J], Chem. Eng. J. (2024) 149776.
[6] Y. Zhang, M. Wu, Y. Wang, et al., Fluorinated TiO2 coupling with α-MnO2 nanowires supported on different substrates for photocatalytic VOCs abatement under vacuum ultraviolet irradiation[J], Appl. Catal. B-Environ. 280 (2021) 119388.
[7] Y. Cheng, H. He, C. Yang, et al., Challenges and solutions for biofiltration of hydrophobic volatile organic compounds[J], Biotechnol. Adv. 34 (6) (2016) 1091–1102.
[8] M.F. Mustafa, X. Fu, Y. Liu, et al., Volatile organic compounds (VOCs) removal in non-thermal plasma double dielectric barrier discharge reactor[J], J. Hazard. Mater. 347 (2018) 317–324.
[9] Z. Lu, L. Guo, Q. Shen, et al., The application of metal–organic frameworks and their derivatives in the catalytic oxidation of typical gaseous pollutants: recent progress and perspective[J], Sep. Purif. Technol. 126772 (2024).
[10] W. Yang, M.Y. Kim, F. Polo-Garzon, et al., CH4 combustion over a commercial Pd/CeO2-ZrO2 three-way catalyst: impact of thermal aging and sulfur exposure[J], Chem. Eng. J. 451 (2023) 138930.
[11] J. Ji, Y. Xu, H. Huang, et al., Mesoporous TiO2 under VUV irradiation: enhanced photocatalytic oxidation for VOCs degradation at room temperature[J], Chem. Eng. J. 327 (2017) 490–499.
[12] Z. Zhang, Z. Jiang, W. Shangguan, Low-temperature catalysis for VOCs removal in technology and application: a state-of-the-art review[J], Catal. Today 264 (2016) 270–278.
[13] Q. Zhou, L. Zhang, J. Chen, et al., Enhanced stable long-term operation of biotrickling filters treating VOCs by low-dose ozonation and its affecting mechanism on biofilm[J], Chemosphere 162 (2016) 139–147.
[14] X. Zhang, B. Gao, R. Rao, et al., Defects materials of institut Lavoisier-125 (Ti) materials enhanced photocatalytic activity for toluene and chlorobenzene mixtures degradation: mechanism study[J], J. Colloid Interface Sci. 660 (2024) 423–439.
[15] M. Sansotera, S. Geran Malek Kheyli, A. Baggioli, et al., Absorption and photocatalytic degradation of VOCs by perfluorinated ionomeric coating with TiO2 nanopowders for air purification[J], Chem. Eng. J. 361 (2019) 885–896.
[16] X. Li, J. Ma, X. Ling, Design and dynamic behaviour investigation of a novel VOC recovery system based on a deep condensation process[J], Cryogenics 107 (30) (2020) 103060.
[17] V.K. Gupta, N. Verma, Removal of volatile organic compounds by cryogenic condensation followed by adsorption[J], Chem. Eng. J. 57 (14) (2002) 2679–2696.
[18] G. Gan, S. Fan, X. Li, et al., Adsorption and membrane separation for removal and recovery of volatile organic compounds[J], J. Environ. Sci. 123 (2023) 96–115.
[19] Z. Petrusová, K. Machanová, P. Stanovský, et al., Separation of organic compounds from gaseous mixtures by vapor permeation[J], Sep. Purif. Technol. 217 (2019) 95–107.
[20] L. Zhu, D. Shen, K.H. Luo, A critical review on VOCs adsorption by different porous materials: species, mechanisms and modification methods[J], J. Hazard. Mater. 389 (2020) 122102.
[21] X. Li, L. Zhang, Z. Yang, et al., Adsorption materials for volatile organic compounds (VOCs) and the key factors for VOCs adsorption process: a review[J], Sep. Purif. Technol. 235 (2020) 116213.
[22] Q. Ke, T. Sun, X. Wei, et al., Economical synthesis strategy of RHO zeolites with fine-tuned composition and porosity for enhanced trace CO2 capture[J], Chem. Eng. J. 359 (2019) 344–353.
[23] Q. Ke, T. Sun, X. Wei, et al., Enhanced trace carbon dioxide capture on heteroatom-substituted RHO zeolites under humid conditions[J], ChemSusChem 10 (21) (2017) 4207–4214.
[24] X. Zhang, S. Ma, B. Gao, et al., Effect of benzoic acid and dopamine hydrochloride as a modulator in the water resistance of Universitetet i Oslo-67: adsorption performance and mechanism[J], J. Colloid Interface Sci. 651 (2023) 424–435.
[25] L. Yang, S. Qian, X. Wang, et al., Energy-efficient separation alternatives: metal–organic frameworks and membranes for hydrocarbon separation[J], Chem. Soc. Rev. 49 (15) (2020) 5359–5406.
[26] S. Lu, R. Han, H. Wang, et al., Three birds with one stone: designing a novel binder-free monolithic zeolite pellet for wet VOC gas adsorption[J], Chem. Eng. J. 448 (2022) 137629.
[27] S. Lu, Q. Liu, R. Han, et al., Potential applications of porous organic polymers as adsorbent for the adsorption of volatile organic compounds[J], J. Environ. Sci. 105 (2021) 184–203.
[28] K. Xiao, H. Liu, Y. Li, et al., Excellent performance of porous carbon from urea-assisted hydrochar of orange peel for toluene and iodine adsorption[J], Chem. Eng. J. 382 (2020) 122997.
[29] A.R. Bagheri, N. Aramesh, F. Sher, et al., Covalent organic frameworks as robust materials for mitigation of environmental pollutants[J], Chemosphere 270 (2021) 129523.
[30] M.B. Poudel, M. Shin, H.J. Kim, Interface engineering of MIL-88 derived MnFe-LDH and MnFe2O3 on three-dimensional carbon nanofibers for the efficient adsorption of cr (VI), pb (II), and as (III) ions[J], Sep. Purif. Technol. 287 (2022) 120463.
[31] M.B. Poudel, G.P. Awasthi, H.J. Kim, Novel insight into the adsorption of cr (VI) and pb (II) ions by MOF derived co-al layered double hydroxide@ hematite nanorods on 3D porous carbon nanofiber network[J], Chem. Eng. J. 417 (2021) 129312.
[32] J. Abdulsalam, M. Onifade, S. Bada, et al., The spontaneous combustion of chemically activated carbons from south african coal waste[J], Combust. Sci. Technol. 194 (10) (2022) 2025–2041.
[33] X. Li, J. Wang, Y. Guo, et al., Adsorption and desorption characteristics of hydrophobic hierarchical zeolites for the removal of volatile organic compounds [J], Chem. Eng. J. 411 (2021) 128558.
[34] T. Wu, Q. Ke, M. Lu, et al., Recent advances in carbon-silica composites: preparation, properties, and applications[J], Catalysts 12 (5) (2022) 573.
[35] L. Fu, J. Zhu, W. Huang, et al., Preparation of nano-porous carbon-silica composites and its adsorption capacity to volatile organic compounds[J], Processes 8 (3) (2020) 372.
[36] B. Dou, J. Li, Y. Wang, et al., Adsorption and desorption performance of benzene over hierarchically structured carbon–silica aerogel composites[J], J. Hazard. Mater. 196 (2011) 194–200.
[37] Z. Han, S. Kong, H. Sui, et al., Preparation of carbon-silicon doping composite adsorbent material for removal of VOCs[J], Materials 12 (15) (2019) 2438.
[38] X. Lu, J. He, J. Xie, et al., Preparation of hydrophobic hierarchical pore carbon–silica composite and its adsorption performance toward volatile organic compounds[J], J. Environ. Sci. 87 (2020) 39–48.